Numerical Modeling of Debris Flow during a Rainfall Induced Landslide at Malin in India

Avinash Sajwan, M.Tech.[1] and Aniruddha Sengupta, Ph.D., AM.ASCE[2]

[1] Graduate Student, Dept of Civil Engg, IIT Kharagpur 721302 India, Email: avinashsajwan.jnv22@gmail.com

[2]Professor, IIT Kharagpur 721302, India, (Corresponding Author) Email: sengupta@civil.iitkgp.ac.in

ABSTRACT

On 30th July 2014, a devastating rainfall induced landslide happened at a place called Malin located 110 km from Pune in West Maharashtra (India) which wiped out an entire village along with a school building and causing nearly 160 casualties. The debris flow at Malin is numerically modeled by discrete element analysis (DEM) using the PFC2D computer software. The results of the numerical analysis in terms of the extent of the debris flow, depth of debris at different locations, movement of debris from different locations, velocity of the debris flow are presented and compared with the information available from field measurements and observations. A reasonably good match between the numerical results and the field observations indicates that the developed numerical methodology can be effectively used to predict the areas affected by debris flows during a landslide.

INTRODUCTION

This paper presents a numerical simulation of a devastating rainfall-induced slope failure and debris flow occurred at a place called Malin using a distinct element method (DEM) as in PFC2D (Itasca 1996). The Malin (N 19º 09' 34" and E 73º 41' 19") is located at an elevation of 760m from mean sea level within the Western Ghat mountain range and 110 km away from the city of Mumbai within the Indian state of Maharashtra (see Fig. 1). The slope failure occurred in the early morning of July 30, 2014 after a few days of continuous rainfall. The debris flow from the slope failure buried the whole Malin village with 44 houses and a school building and claimed the lives of 160 villagers.

Figure 1. Location of Malin on a map of India.

A number of researchers (Dey & Sengupta 2018; Meshram 2016; Naykodi et al. 2016; Ering et al. 2015) have looked into the Malin landslide in the recent past. Most of the published literatures describe parametric studies on the possible triggering factors responsible for the landslide at Malin. Dey & Sengupta (2018) have looked into the pore water pressure generation and matric

suction reduction within the Malin slope with rainfall intensity and duration. They have modelled the day by day reduction of the safety factor of the Malin hill slope with recorded rainfall event leading to the disaster.

The present study attempts to numerically model the debris flow that followed the uphill slope failure at Malin using distinct element method and compares the results with the field observations described in the literature.

Geology and Profile of Malin

The surrounding areas of Malin village consist of solidified basalt formed by lava flows in prehistoric ages. The top surface of the slope is deeply weathered basalt and may be classified as silty clay with loose gravels. The colour of the rock is dark grey, while the surface material is grey to red.

The rainfall data of Malin from 21st to 30th July 2014 is given by Dey & Sengupta (2018) which indicates that the rainfall intensity increased several folds from 28th July onward with the maximum on 29th and 30th July and the landslide was triggered on early morning of 30th July. There has been no doubt about the role of the very heavy rainfall in the last two days on the triggering of the Malin landslide.

The cross-sectional profile of the Malin slope is shown in Fig. 2. The entire hill slopes may be divided into four zones depending upon the inclination. A small stream (locally called 'nala') is located at the foothill of Malin. It may be noted that the lower part of Zone 2 in Fig. 2, where the main road and 46 houses are located, has a very gentle slope of 10º. As reported by Ering et al. (2015) and Meshram (2016), the slope failure was initiated at the lower part of Zone 4 and continued through the entire Zone 3 and the upper part of Zone 2. The debris moved through the lower part of Zone 2, where the main road and the Malin village were located.

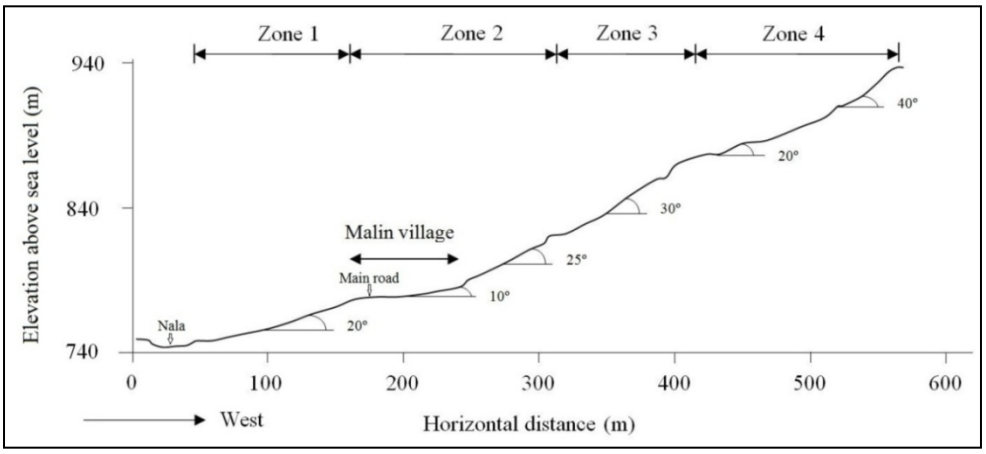

Figure 2. Cross sectional profile of Malin slope.

Distinct element method

In this study distinct element analyses are performed to numerically model the debris flows at Malin. The inter-particulate interactions within a granular material can be better understood if

they are studied as a discontinuous system, as at some level from macroscopic to microscopic, these materials are discontinuous. The particle flow code (PFC) of Itasca Consulting Group Inc. (1996) is based on the distinct element method (hence forth to be referred as DEM). The distinct element method is originally proposed by Cundall and Strack (1979) and it is a subset of discrete element method. It simulates the physical interaction of particles within a body with finite mass. In the recent past, the DEM has been successfully utilized in the study of debris flow during a landslide (Su et al. 2019; Zhao 2014; Li et al. 2012; Legros 2002). The representation of solids, inter-particulate contacts and contact recognition are three aspects that separate a DEM from other numerical methods. The discontinuous medium (body) in DEM is represented by rigid or deformable solids, like, balls, walls, etc. The balls are represented by disks of unit thickness in 2D and spheres in 3D. The contact mechanics is embodied in particle interaction laws where it is assumed that, all the deformations occur at the contacts between the rigid particles. Each contact stores a force (Fc) and a moment (Mc) that act at the contact location that are updated by the particle interaction law by utilizing the positions and relative motion of the two pieces. The particle interaction law is referred to as a contact model. The translational and the rotational displacements of the particles are calculated by explicitly integrating the governing differential equations based on Newton's laws of motion. In describing the stated dynamic process, the time step selected is so small that the velocity and the acceleration are assumed to be constant within each time step. The equations of motion are solved numerically for balls/clumps by second order velocity Verlet algorithm (Verlet, 1967).

In the DEM, the velocity ($\vec{v}$) and position ($\vec{x}$) of a particle at a time, t with a time step, Δt, are updated by Velocity Verlet algorithm as:

$$\vec{v}^{(t+\Delta t/2)} = \vec{v}^{(t)} + \frac{1}{2}\left(\frac{\vec{F}^{(t)}}{m} + \vec{g}\right)\Delta t \quad (1)$$

$$\vec{x}^{(t+\Delta t/2)} = \vec{x}^{(t)} + \vec{v}^{(t+\Delta t/2)}\Delta t \quad (2)$$

$$\vec{v}^{(t+\Delta t)} = \vec{v}^{(t+\Delta t/2)} + \frac{1}{2}\left(\frac{\vec{F}^{(t+\Delta t)}}{m} + \vec{g}\right)\Delta t \quad (3)$$

Where, m is particle mass, $\vec{g}$ is body force acceleration vector. $\vec{F}$ is the resultant force acting on a body.

In the same way, the recent angular acceleration ($\vec{\alpha}$) is used to update the angular velocity ($\vec{\omega}$) using velocity Verlet algorithm for rotational motion.

In PFC, the interactions of the particles are governed by contact models. In the present study, a 'rolling resistance linear model' and a 'linear parallel bond model' have been used.

The rolling resistance linear model incorporates torque acting on contacting particles to counteract the rolling motion. The friction with non-tensile behavior is represented by linear component and viscous behavior is enacted by the dashpot assembly (Ai et al., 2011; Wensrich, 2012). The friction coefficient, μ, is used to ensure a Coulomb limit on the shear force to accommodate the slip as follows.

$$(F_s^l)_{t+\Delta t} = (F_s^l)_t + k_s * \delta_s \quad ; \quad (F_s^l)_{max} = -\mu F_n^l \tag{4}$$

Where, $(F_s^l)_{t+\Delta t}$, $(F_s^l)_t$, $(F_s^l)_{max}$ are the shear component and the limiting value of a linear force at a different time interval, k_s is the shear stiffness, μ is a friction coefficient and δ_s is the incremental shear displacement.
The linear normal force at t+Δt is expressed as:

$$(F_n^l)_{t+\Delta t} = (F_n^l)_t + k_n * \delta_n \quad ; \quad (F_n^l) = k_n * g_s \tag{5}$$

Where, F_n^l, $(F_n^l)_{t+\Delta t}$ are a normal linear force at a different time interval, k_n is the normal stiffness, δ_n is the incremental relative displacement, and g_s is the overlap distance.

The moment at t+Δt is given as:

$$(M^r)_{t+\Delta t} = (M^r)_t + k_r * \Delta\theta_b \quad ; \quad (M^r)_{max} = \mu_r \bar{R} F_n^l \tag{6}$$

Where, $(M^r)_{t+\Delta t}$, $(M^r)_t$ are rolling resistances at a different time interval and $(M^r)_{max}$ is its maximum value. k_r is a rolling stiffness, μ_r is a rolling friction coefficient. $\Delta\theta_b$ is the relative bend-rotation increment. The relationship between shear stiffness and rolling stiffness may be expressed as:

$$k_r = k_s * \bar{R}^2 \quad ; \quad \frac{1}{\bar{R}} = \frac{1}{R^1} + \frac{1}{R^2} \tag{7}$$

Where, R^1, R^2 are radii of interacting pieces and $\bar{R}$ is the effective radius.

In the Linear Parallel Bond Model, a bond provides the mechanical behavior of a cementing material between the contacting particles that acts parallel to the linear model component and can transmit both the force and the moment. The relative motion between the bodies at the parallel bonded contact develops a force and a moment that can be related to the stresses acting within the bond material. The bond is broken, if stresses exceed a specific limit given by the bond strength.

The force-displacement law for the linear parallel bond model is given by

$$F_c = F^l + F^d + \bar{F} \; ; \quad M_c = \bar{M} \tag{8}$$

Where, F^l, F^d and $\bar{F}$ are the linear force, the dashpot force and the parallel bond force. $\bar{M}$ is the parallel bond moment.

The linear and the dashpot forces are updated as in the linear model, described before. The parallel bond force is resolved into a normal force ($\bar{F}_n$) and a shear force ($\bar{F}_s$) as shown in Eq. (11). The moment is resolved into a twisting ($\bar{M}_t$) moment and a bending moment ($\bar{M}_b$) as

$$\bar{F} = -\bar{F}_n \hat{n}_c + \bar{F}_s \; ; \; \bar{M} = \bar{M}_t \hat{n}_c + \bar{M}_b = \bar{M}_b \; ; (\bar{M}_t = 0 \; for \; 2D) \tag{9}$$

The cross-sectional properties of a bond for the 2D model (t =1) are updated as:

$$\bar{R} = \min(R^1, R^2)\ ;\ \bar{A} = 2\bar{R}t\ ;\quad \bar{I} = (2/3)t\bar{R}^3 \tag{10}$$

Where, $\bar{R}$ is effective radius and $R^1$and R^2 are the radii of contacting pieces, $\bar{A}$ is the cross sectional area, t is thickness and $\bar{I}$ is the moment of inertia of a bond cross section.

The moment component of the parallel bond moment at t+Δt is calculated as:

$$(\bar{M}_b)_{t+\Delta t} = (\bar{M}_b)_t - \bar{k}_n * \bar{I} * \Delta\theta_b \tag{11}$$

Where, $(\bar{M}_b)_{t+\Delta t}$, $(\bar{M}_b)_t$ are the moment components of the parallel bond moment at different time intervals and $\Delta\theta_b$ is the relative bend-rotation increment.

Modeling of debris flow at Malin during 2014 rainfall induced slope failure

The numerical modeling of the debris flow that followed after the 2014 rainfall induced slope failure at Malin, is performed using DEM in PFC2D. As DEM is still not very common choice of analysis, it has been briefly described separately, beforehand. The material properties of the slide materials and zones above the residential area are obtained from Meshram (2016) and Ering and Babu (2016) and shown in Table 1. These data are based on the laboratory tests on the representative soil samples collected from the slide area.

Table 1. Malin landslide's soil properties (Ering and Babu, 2016).

Parameter	Value	Parameter	Value
Dry density (kg/m^3)	1336	Bulk density (kg/m^3)	1700
Specific gravity	2.56	Porosity	0.15
Cohesion (kPa)	36	Friction angle (°)	22
Young's modulus (MPa)	1.73	Poisson's ratio	0.44
Grain size analysis	Silty clay with sand	Moisture content (%)	27.3

The model parameters for DEM are somewhat difficult to determine. In the present study, they are estimated by numerically modeling (in 2D) a series of laboratory triaxial drained tests at all around confining pressures of 50, 100 and 150kPa. In each case, the soil sample is consolidated and then sheared to failure. The stress-strain, radial strain-axial strain curves and the Mohr-Coulomb failure envelope predicted by the DEM simulations of the triaxial tests for the soil at Malin are shown in Fig. 3. Table 3 delineates the 'arrlinear' model parameters for the simulation of debris flow at Malin. Table 4 shows the 'linear pbond' model parameters for Malin soil. It may be noted that the model parameters, such as, activity distance, friction coefficient, and adhesive force are responsible for the resulting cohesion and the friction angle in the DEM model. These parameters are calibrated to obtain the same values given in Table 1.

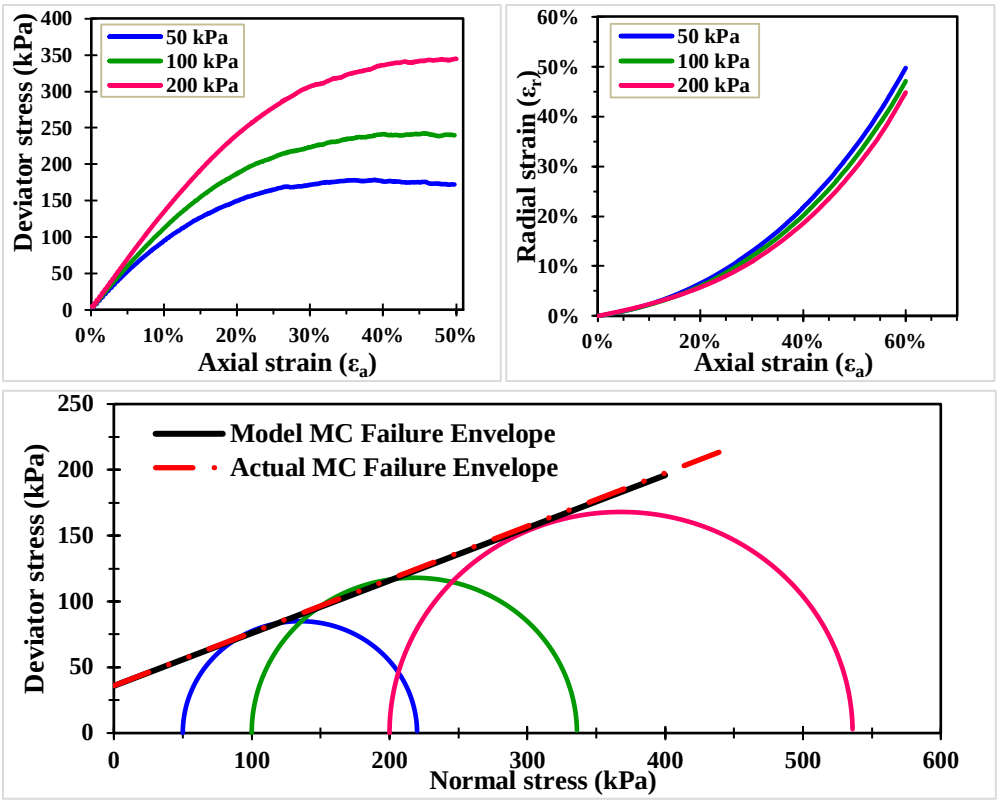

Figure 3. DEM triaxial results of the Malin soil: (a) deviator stress vs. axial strain, (b) radial vs. axial strains, (c) Mohr-Coulomb representation of stress condition at failure.

Table 2. Parameters of the 'arrlinear' model from the triaxial tests.

Parameter	Value	Parameter	Value
Density (den)	1570 kg/m^3	Porosity (n)	0.15
attractive force (arr_f0)	0.555 N	Attractive distance (arr_d0)	3 mm
Friction (fric)	0.3	Normal damping (dp_nratio)	0.2
Minimum particle size (dmin)	2 mm	Maximum particle size (dmax)	4 mm
Effective modulus (emod)	2 MPa	Stiffness ratio (kratio)	2.0

The unique parameters of the 'arrlinear' model (see Table 2), such as, 'arr_f0', represent the attractive force added to each particle and equals to 375 times the weight of an average particle. The parameter 'arr_d0' represents the distance up to which this attractive force is active. Other quantities are basic parameters of the model. The unique parameters of the 'linear pbond' model (Table 3) such as 'pb_emod,' 'pb_kratio,' 'pb_fa,' and 'gap' represent effective modulus, stiffness ratio, friction angle and the activity distance of the bond, respectively. The other quantities are basic model parameters. As may be observed from Fig. 3, the predicted Mohr-Coulomb failure/yield envelope is matching with that from the actual laboratory tests on Malin soil.

Table 3. The ‘linearpbond’ model parameters for Malin soil.

Parameter	Value	Parameter	Value
Density (den)	1570 kg/m^3	Porosity (n)	0.15
Cohesion (pb_coh)	27 kPa	Tensile (pb_tensile)	153 kPa
Friction (fric)	0.3	Normal damping (dp_nratio)	0.2
Minimum particle size (dmin)	0.6 m	Maximum particle size (dmax)	1.0 m
Effective modulus (emod)	20 MPa	Stiffness ratio (kratio)	2.0
Activity distance (gap)	0.1 m	Bond friction (pb_fa)	10°
Bond modulus (pb_emod)	20 MPa	Bond stiffness ratio (pb_kratio)	2.0

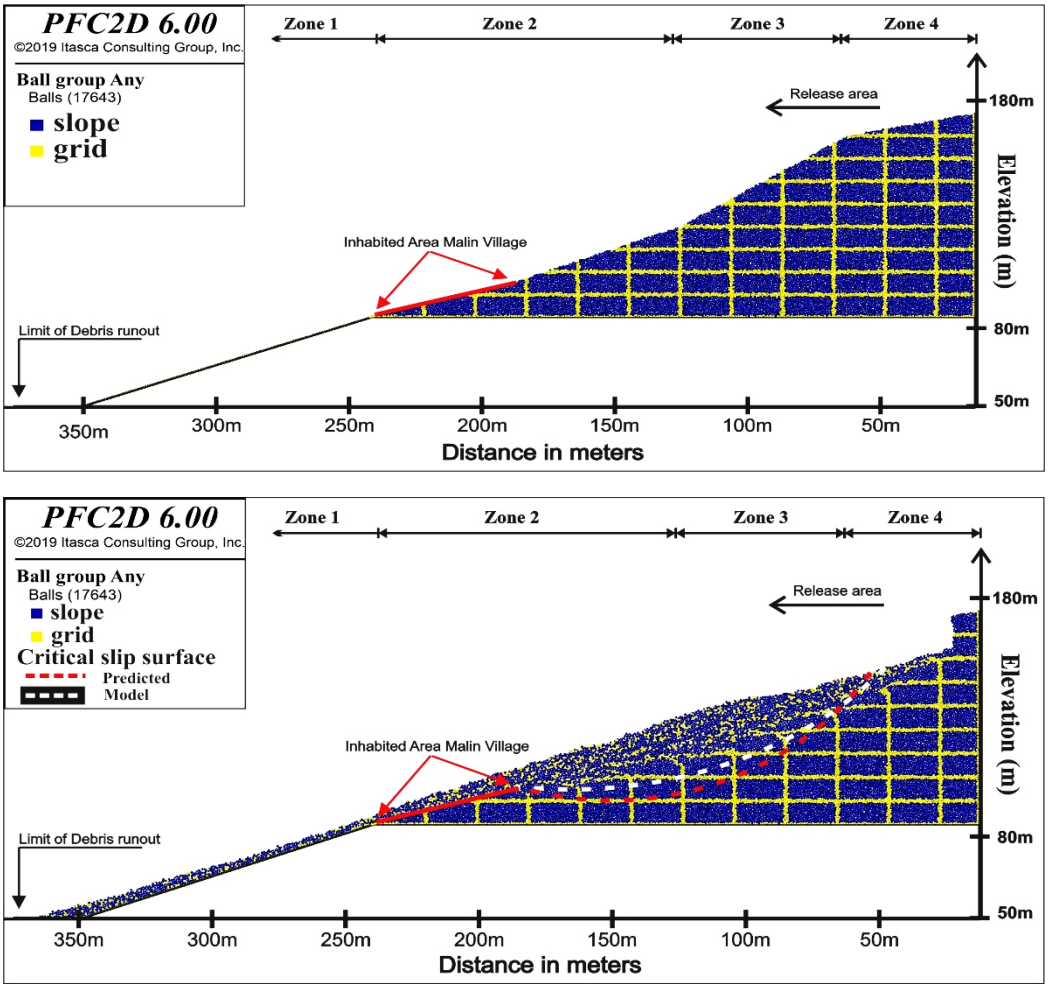

Figure 4. Predicted deformations of Malin slope: (a) Pre-failure, (b) Post-failure.

Figure 4 shows the predicted deformations of the Malin slope before and after the landslip. The Malin village area on the slope is shown with a red line in the figure. In the DEM model, the saturation of the debris and the slope materials, and the corresponding fluid-forces has been incorporated. A grid is generated on the slope cross section by grouping and coloring the

particles according to their initial position to visualize the deformation pattern and the slip surface. The critical slip surface with a factor of safety 0f 0.709 given by Dey and Sengupta (2018) based on their slope stability analyses, considering progressive saturation of the Malin slope with the seepage of rainwater through the initially unsaturated soil, is shown in red dashed line. The deformations of the grids in Fig. 4 reveal that the slip surface predicted by the present DEM analyses is very close to the reported slip surface by Dey and Sengupta (2018) and it also matches with the field observations reported in the literature.

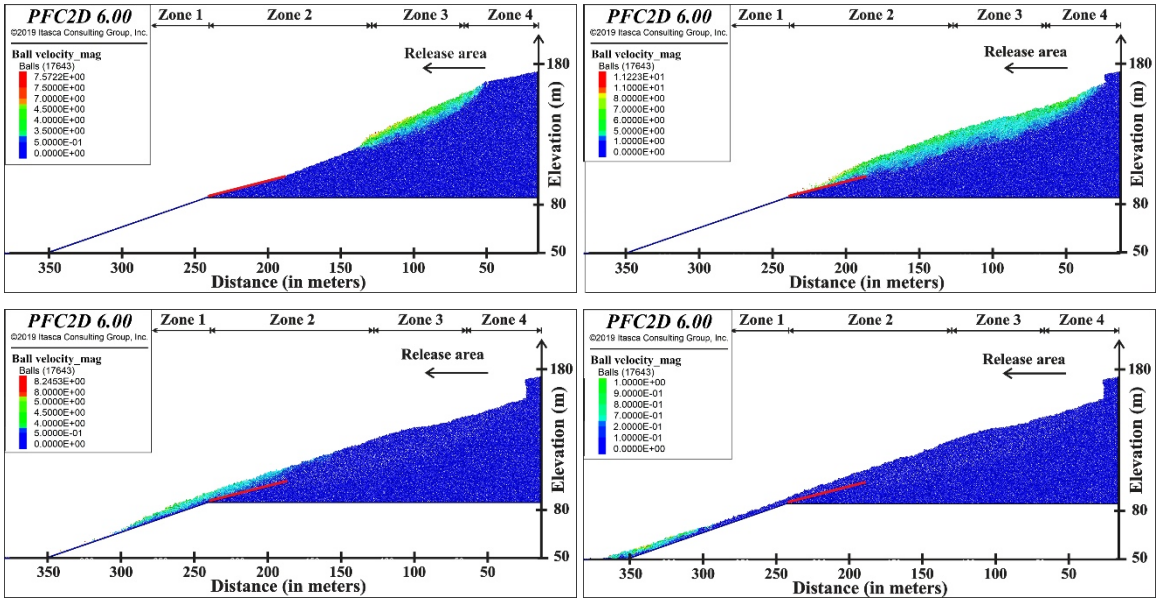

Figure 5. Evolution of debris flow in Malin at time: (a) T=10s, (b) T=25s, (c) T=50s, (d) T=100s.

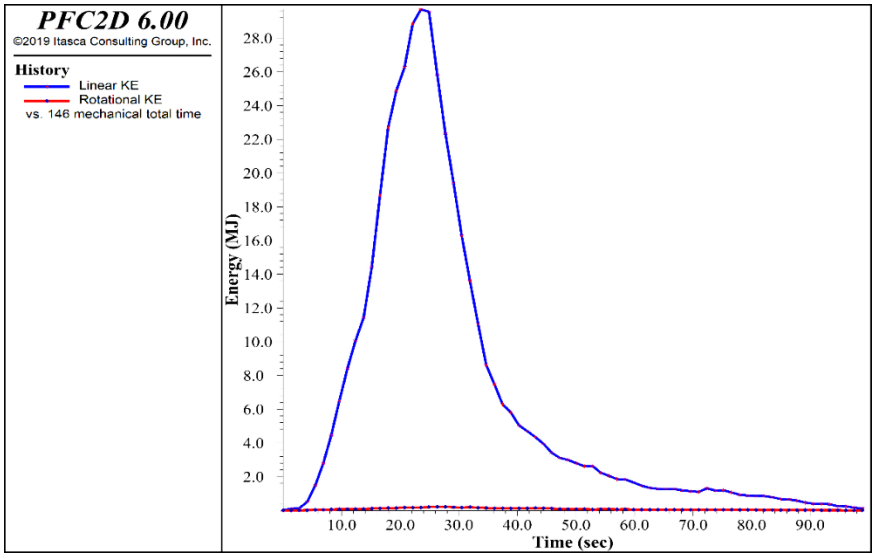

Figure 6. Kinetic energy of the debris flow from the DEM analyses of the Malin landslide.

The material flow velocity in the different zones at different times is shown in Fig. 5. The figure reveals that the landslide initiates from Zone 3, which has the steepest slope. The accelerating

high velocity flow reaches Zone 2 and scours the base material increasing the mass of the debris flow. The rampaging debris flow possessing tremendous kinetic energy (see Fig. 6), impacts the Malin village after twenty seconds from the start of the landslip. The rotational component is found to be insignificant compared to the translational component of the total kinetic energy, suggesting that the sliding and the slipping of the slope (debris) materials is the dominant movement. The loss of energy results in the deposition of the debris in Zones 1 and 2 with an average deposition depth of 6 to 8m over the Malin village. This depth of deposition of debris at Malin village is very close to the 7m estimated by Ering et al. (2015). The stresses and the displacements of the particles are also tracked at different locations on the Malin slope. The particles from the landslide initiation area (Zone 3) have traveled the maximum distance as compared to the particles from Zones 2 and 4. The eroded particles from Zone 2 are beneath the massive moving debris leading to their early deposition. The materials from Zone 4 lie in the tail region following the materials from Zone 3.

CONCLUSIONS

The slope failure and the debris flow after an incessant rainfall at Malin has been modelled by DEM using PFC2D. The location of the slip surface predicted by DEM is found to be reasonably close to the failure surface reported in the literatures. The numerical model indicates that the Malin village would be buried under 6-8m of debris originating from the upslope areas. This value is also found to be very close to the 7m of debris at Malin village area reported in the literatures. The present analyses indicate that the sliding and the slipping of the slope (debris) materials is the dominant movement as the rotational component is found to be insignificant.

ACKNOWLEDGEMENT

This study is a part of an ongoing Indo-Norway collaborative project on landslide hazard assessment in Sikkim sponsored by Ministry of Earth Sciences (MoES), Govt of India, New Delhi, vide MoES/Indo-Nor/PS-2/2015 dtd 26.04.2017.

REFERENCES

1. Ai J., Chen J.F., Rotter J.M. and Ooi J.Y. (2011). “Assessment of rolling resistance models in discrete element simulations.” *Powder Technology*, 206(3), 269-282.
2. Cundall P.A. and Strack O.D. (1979). “A discrete numerical model for granular assemblies.” *Geotechnique*, 29(1), 47-65.
3. Dey N., Sengupta A. (2018). “Effect of rainfall on the triggering of the devastating slope failure at Malin, India.” *Natural Hazards*, 10.1007/s11069-018-3483-9.
4. Ering P. and Babu G.S. (2016). “Probabilistic back analysis of rainfall induced landslide-A case study of Malin landslide, India.” *Eng. Geol.*, 208, 154-164.
5. Ering P., Kulkarni R., Kolekar Y., Dasaka S.M. and Babu G.S. (2015). “Forensic analysis of Malin landslide in India.” In *IOP conference series: earth and environmental science*, 26(1), 01204.
6. Itasca Consulting Group Inc. (1996). “PFC2D- Particle Flow in Two-Dimensions, Version 6.0, User Manual.” Minneapolis, Minnesota, USA.
7. Legros F. (2002). “The mobility of long-runout landslides.” *Eng. Geol.*, 63(3-4), 301-331.

8. Li W.C., Li H.J., Dai F.C. and Lee L.M. (2012). “Discrete element modeling of a rainfall-induced flowslide.” *Eng. Geol.*, 149, 22-34.
9. Meshram S. (2016). “Investigations of the causes of landslide at Malin and some preventive measures.” *J. Geotech. Stud.*, 1(2), 1–14.
10. Naykodi A., Takalkar O., Bhor A., Jadav K., SA N. (2016). “A review paper on slope stability analysis of Malin landslide.” In: *TECHNOPHILIA-2016*, Jaihind Polytechnic, Kuran, India, 101–106.
11. Su H., Fu Z., Gao A. and Wen Z. (2019). “Numerical Simulation of Soil Levee Slope Instability Using Particle-Flow Code Method.” *Natural Hazards Review*, 20(2), 04019001.
12. Verlet L. (1967). “Computer ‘experiments’ on classical fluids. I. Thermodynamical properties of Lennard-Jones molecules.” *Physical review*, 159(1), 98-103.
13. Wensrich C.M. and Katterfeld A. (2012). “Rolling friction as a technique for modelling particle shape in DEM.” *Powder Technology*, 217, 409-417.
14. Zhao T. (2014). “Investigation of Landslide-induced Debris Flows by the DEM and CFD.” Doctoral dissertation, University of Oxford, UK.